Confinement regime in self-assembled InAs/InAlGaAs/InP quantum dashes determined from exciton and biexciton recombination kinetics

Ł. Dusanowski, P. Mrowiński, M. Syperek, J. Misiewicz, A. Somers, S. Höfling, J. P. Reithmaier, and G. Sęk

Confinement regime in self-assembled InAs/InAlGaAs/InP quantum dashes determined from exciton and biexciton recombination kinetics

Ł. Dusanowski,[1,2] P. Mrowiński,[1] M. Syperek,[1] J. Misiewicz,[1] A. Somers,[2] S. Höfling,[2,3] J. P. Reithmaier,[2,4] and G. Sęk[1]

[1]*Laboratory for Optical Spectroscopy of Nanostructures, Department of Experimental Physics, Faculty of Fundamental Problems of Technology, Wrocław University of Science and Technology, Wybrzeże Wyspiańskiego 27, 50-370 Wrocław, Poland*
[2]*Technische Physik, University of Würzburg, Wilhelm-Conrad-Röntgen-Research Center for Complex Material Systems, Am Hubland, D-97074 Würzburg, Germany*
[3]*School of Physics and Astronomy, University of St. Andrews, North Haugh, KY16 9SS St. Andrews, United Kingdom*
[4]*Institute of Nanostructure Technologies and Analytics (INA), CINSaT, University of Kassel, Heinrich-Plett-Str. 40, 34132 Kassel, Germany*

The exciton and biexciton confinement regimes in strongly anisotropic epitaxial InAs nanostructures called quantum dashes (QDashes) embedded in an $In_{0.53}Ga_{0.23}Al_{0.24}As$ matrix, which is lattice-matched to InP(001) substrate, have been investigated. For that purpose, we have performed low-temperature spatially and polarization-resolved photoluminescence and time-resolved photoluminescence measurements on a set of single QDashes. The main conclusions are drawn based on the experimentally obtained distribution of the ratio between the exciton and biexciton lifetimes. We have found that a majority of QDashes for which the abovementioned ratio falls into the range of 1.2 ± 0.1–1.6 ± 0.1 corresponds to the so called intermediate confinement regime, whereas for several cases, it is close to 1 or 2, suggesting reaching the conditions of weak and strong confinement, respectively. Eventually, we support this data with dependence of the lifetimes' ratio on the biexciton binding energy, implying importance of Coulomb correlations, which change significantly with the confinement regime. *Published by AIP Publishing.* https://doi.org/10.1063/1.5005971

The properties of a Coulomb-correlated electron-hole pair (a neutral exciton) and its derivatives (a negatively or positively charged exciton or biexciton) confined in self-assembled semiconductor quantum dots (QDs) still remain one of the major research areas in physics of low dimensional semiconductor structures. It is of particular relevance to both, fundamental physics and applications, where an exciton or other charge complexes can define functionality of a QD-based device. Only recently, by utilizing a dark exciton state confined in a QD, generation of photonic cluster states of entangled photons was demonstrated[1] which is promising for fault-tolerant implementation of measurement-based quantum computation.[2]

Among many QD material systems, those utilizing the InP(001) substrate play a particular role. First, the substrate is suitable for many currently used technological processes that allow fabricating a final device. Second, the deposition of InAs on InP can lead to the formation of QD-like structures with the ground state exciton emission falling into the telecom bands. Thus, it opens the application potential of InAs on InP QDs for sources of single photons,[3–8] entangled photon pairs,[9] or cluster states dedicated to quantum data processing schemes compatible with short and long-haul silica-fiber-based transmission lines. Following this approach, InAs/InP QDs have been shown to be efficient and pure single photon emitters at wavelengths including both the second[10–12] and third[4,8,13–15] telecom windows, being a direct competitor to InAs QDs grown on InGaAs/GaAs metamorphic buffers.[16,17] High extraction efficiencies up to 46%

(Ref. 18) and Purcell enhancement of the spontaneous emission rate as large as 5[8] have been already reported by successfully embedding InAs/InP QDs into different kinds of optical resonator structures, including photonic crystal[8,12,19] and micropillar[20] cavities or optical horn structures.[13] By utilizing such a QD system, 120 km range fiber-based single photon quantum key distribution was demonstrated,[15] and first two-photon interference measurements at telecom wavelength were reported, showing single photons with indistinguishabilities of 0.18.[18]

Despite these advantages, the control of properties from a dot to dot of an inhomogeneous ensemble of the InAs on InP system remains challenging. The growth of InAs nanostructures on the technologically important InP(001) substrate leads to the formation of strongly in-plane asymmetric and large nano-islands (called quantum dashes—QDashes) instead of more common in-plane symmetric QDs.[21–24] These unique objects are preferentially elongated and aligned along the [1–10] crystallographic direction and are quite non-uniform in the length, size, internal strain, and exhibit irregularities in their morphology.[25] Although some of the exciton and biexciton properties of single InAs/InP(001) QDashes are already known,[26–29] they are not yet fully understood. For instance, a still open question is related to the electron-hole pair confinement regime in QDashes that directly defines, e.g., the kinetics of the exciton and biexciton decay, or affects significantly the exciton and biexciton binding energies. Moreover, it is also important if a specific confinement regime can be treated as a general property of such

large and non-uniform objects. This information is missing in the literature, and this work aims at filling up this gap.

We have used a combination of spatially resolved, time-integrated, and time-resolved photoluminescence techniques to measure and identify emission from exciton (X) and biexciton (XX) states in many InAs QDashes. The X and XX emission lines of the same QDash have been recognized by tracing the emission intensity of excitonic complexes with the excitation power and by polarization-resolved microphotoluminescence (μPL), that provides information about the fine structure splitting and the biexciton binding energy for selected biexciton-exciton (XX-X) pairs. Subsequently, a time-resolved microphotoluminescence (μTRPL) measurement has been performed on each of the XX-X pairs to analyze the emission rates as a function of the emission energy. In addition, a relation between the XX-X decay ratio and the biexciton binding energy as a probe of Coulomb correlations has been analyzed.

The investigated QDash structures were grown in a gas source molecular beam epitaxy system on an S-doped InP(001) substrate. The QDash layer is surrounded by 200 nm (bottom) and 100 nm (top) thick In$_{0.53}$Ga$_{0.23}$Al$_{0.24}$As barriers, lattice-matched to InP. Due to the atoms' surface diffusion anisotropy, the epitaxially formed nanostructures are significantly elongated in one of the in-plane directions (preferentially [1–10]).[21] The typical lateral dimensions of QDashes under this study are about 16 nm in width and between 50 and hundreds of nanometers in length, whereas their height is on the order of 3 nm, with triangular or lens-like cross-sections.[23,30] Since the planar density of QDashes is rather high (above 10^{10} cm^{-2}), a combination of electron beam lithography and etching has been used to process the so called mesa structures on the surface, with different sizes to resolve the emission from single QDashes out of an inhomogeneous ensemble. In general, due to the high planar density of dashes, tunneling effects between the neighboring objects would seem to be feasible. However, we have found that the quantum-mechanical coupling can be neglected in case of strongly inhomogeneous ensemble of QDashes,[31] which is the case for the self-assembled InAs/InP system considered here.

Mesa structures have been fabricated in a form of cuboids with rectangular in-plane shape and having 2:1 size aspect ratio, with longer axis aligned along the [1–10] direction, corresponding to the QDashes elongation axis. It must be mentioned that due to the use of Al-containing barriers, the etched mesa sidewalls are susceptible to oxidation, which can deteriorate their optical properties. The dashes located in the sidewalls vicinity are expected to be the ones with significantly decreased radiative efficiency (due to expected increased concentration of non-radiative recombination centers) and larger emission line broadening (due to sidewalls charge fluctuations and hence enhanced spectral diffusion). Therefore, for the current studies, only narrow and intensive lines have been selected, which should efficiently exclude dashes affected by oxidation at the sidewalls.

For all the experiments, the sample was kept in a liquid-helium continuous-flow cryostat at T = 5 K. The μPL and μTRPL measurements have been performed using two independent setups, both providing the spatial resolution on the order of a single μm. In the case of power-dependent and

polarization-resolved μPL, the sample was excited with the continuous-wave 660 nm line of a semiconductor diode laser, and optical response was analyzed by a 1-m-focal-length single-grating monochromator combined with a liquid nitrogen-cooled InGaAs-based linear detector, providing the overall spectral resolution of $\sim$20 μeV. For the μTRPL measurements, the structure was excited non-resonantly by a train of 160 fs pulses generated by a mode-locked Ti:Sapphire laser at a repetition frequency of 76 MHz, and 830 nm photon wavelength (non-resonant excitation above the InP band gap). In this case, a 0.3-m-focal-length monochromator was used as a spectral filter ($\sim$100 μeV resolution), the outputs of which were equipped with a fiber-coupled NbN superconducting single photon detector with >15% of quantum efficiency and 10 dark counts/s in the 1.3–1.55 μm spectral range or a streak camera of enhanced sensitivity in the infrared. The overall temporal resolution of the μTRPL setup was $\sim$80 ps.

The selection process of the QDash emitters for further analysis and experiments is performed for the 550×275 nm^2 sized mesas, which were found to provide a good spectral separation between detected emission lines and which appeared also to be usually insignificantly affected by the sidewalls-related spectral diffusion processes. As mentioned earlier, the assignment of excitonic complexes is based on excitation power dependence and polarization-resolved μPL measurements in a manner similar as performed in our earlier studies and utilizing already acquired knowledge on the expected binding energies of particular complexes.[27,29] Examples of such μPL spectra recorded for two dash nanostructures denoted as QDash1 and QDash2 are presented in Figs. 1(a)–1(d), respectively. The X and XX assigned spectral lines at energies of 852.2 meV (856 meV) and 849.25 meV
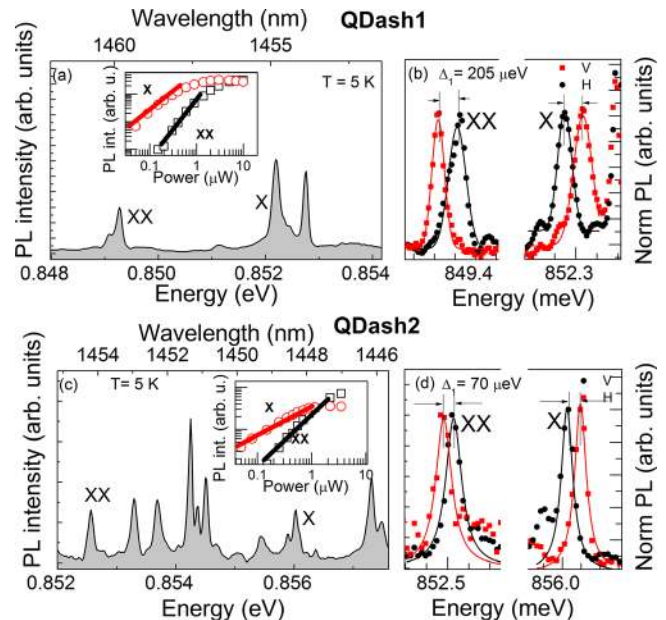

FIG. 1. (a) and (c) An example of the microphotoluminescence spectrum at T = 5 K from the 550×275 nm^2 mesa structure containing InAs/In$_{0.53}$Ga$_{0.23}$Al$_{0.24}$As/InP QDashes. The X and XX spectral features denote exciton and biexciton emissions from the same QDash. Inset: The excitation power dependence of PL intensity emission from the X and XX. (b) and (d) Two orthogonally polarized components of the X and XX emission (red points along [110], black points along [1-10]), demonstrating correlation between two investigated emissions.

(852.5 meV) correspond to the exciton and biexciton emission processes from the same emitter—QDash1 (QDash2), respectively. The insets in Figs. 1(a) and 1(c) show the excitation power dependence of the X and XX lines intensity, with characteristic intensity evolution with excitation power (close to linear or quadratic dependence for exciton and biexciton, respectively). To support the lines' assignment, linear-polarization resolved μPL experiments is performed, revealing fully opposite in phase linear polarization dependences of the X and XX emission and equal energy splittings of both X and XX lines, with linear polarizations aligned along [110] and [1–10] directions, taken from full-rotation polarization series [Figs. 1(b) and 1(d)]. In the presented examples, the fine structure splitting is 205 ± 10 μeV and 70 ± 10 μeV, while the biexciton binding energy of $\sim$2.95 meV and $\sim$3.5 meV is obtained for QDash1 and QDash2, respectively. It is important to note that all the selected and further considered XX-X pairs exhibit a similar behavior as in the presented example, varying only in the fine structure splitting and the biexciton binding energy.

Time-resolved μPL experiment can provide essential information for the initial interpretation of the confinement regime in QDashes. Figures 2(a) and 2(b) present two pairs of μTRPL traces recorded for two different QDashes (the same as in Fig. 1), plotted in the semi-logarithmic scale and recorded separately for a selected pair of XX-X lines, assigned as X and XX. Both traces have been measured with non-resonant excitation and the average pump power of P $= 2$ μW (measured outside the cryostat), which is high enough to observe the XX line and low enough to limit the XX-X cascade refiling process, which is usually visible in μTRPL traces at higher excitation densities.[27] Each of the μTRPL traces exhibits a monoexponential decay, preceded by a setup resolution limited PL rise. The fitting procedure (dashed lines) performed for QDash1 (QDash2) gave the decay time constants of 3.00 ± 0.05 ns (1.63 ± 0.05 ns) and 1.60 ± 0.05 ns (1.35 ± 0.05 ns) for X and XX emission, respectively. The confidence interval for the obtained values has been estimated to be 50 ps, as generated by the fitting procedure. With these numbers, one can obtain the essential parameter for further analysis, namely, the exciton to biexciton decay times' ratio τ_X/τ_{XX}. In the considered case, it equals to 1.9 ± 0.1 and 1.3 ± 0.1 for QDash1 and QDash2, respectively. At this point, it is worth mentioning that due to significantly polarized emission from QDashes, in time-resolved experiments, we probe mainly the [1–10] direction polarized emission.

The τ_X/τ_{XX} value contains the information about the exciton confinement regime in a quasi-0D potential, usually described by the two limiting cases: strong and weak confinement. In the strong confinement regime, the X and XX can be described by a simple product of the electron and hole wave functions, which can be realized in a system where the quantization energy exceeds the binding energy of both complexes.[32] In such a case, Coulomb correlations and, in particular, the configuration mixing contribution to the excitonic states only slightly perturb the final exciton and biexciton wavefunctions. In the most simplified picture, the biexciton recombination can be treated as an independent emission process of two non-interacting excitons, following the number of allowed decay channels, i.e., the biexciton lifetime should then be two times shorter than the exciton one and thus $\tau_X/\tau_{XX} = 2$. In the opposite case, i.e., in the weak confinement regime, the Coulomb interactions and configuration mixing become significant with respect to quantization energy and led to the formation of strongly correlated complexes. In such a case, excitonic wavefunctions are more bulk-like and extend across the dot volume, leading to an increased X decay rate. For the XX recombination, no increase in the recombination rate is expected, as the exciton final state after the recombination suppresses the enhancement, so that in the ultimate case $\tau_X/\tau_{XX} = 1$.[32,33] Between the limits of strong and weak confinement regimes, there is a range of the system parameters which corresponds to the so called intermediate confinement, where $1 < \tau_X/\tau_{XX} < 2$ is expected. It is important to note that the extreme values of the τ_X/τ_{XX} ratio are valid under the assumption of a long spin flip relaxation process within the fine structure of an exciton (i.e., its bright and dark states), exceeding significantly the radiative recombination lifetime.[33] The value of lifetimes ratios obtained in the discussed examples $\tau_X/\tau_{XX} = 1.9 \pm 0.1$ for QDash1 and 1.3 ± 0.1 for QDash2 suggests that the considered structures might be classified in two different confinement regimes based on biexciton cascade kinetics. QDash1 fits more to the strong confinement regime due to τ_X/τ_{XX} close to 2, while in the case of QDash2, the emission kinetics seems to be strongly affected by the Coulomb interactions and configuration mixing, lowering τ_X/τ_{XX} down to 1.3 and placing it in the intermediate confinement regime.
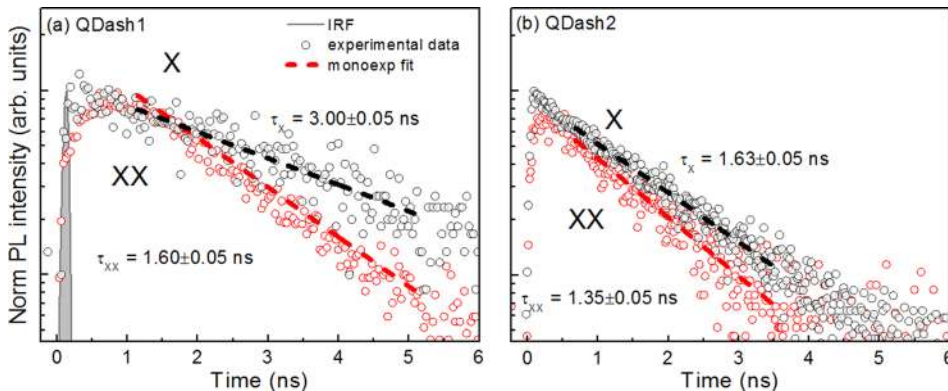

FIG. 2. (a) and (b) Examples of time-resolved PL traces (black solid lines) at T $= 5$ K recorded for X and XX emission lines for QDash1 and QDash2 (detailed in Fig. 1). Dashed lines indicate a single exponential fit to experimental data. The instrumental response function (IRF) of the μTRPL system is shown by the grayed area and characterized by the full width at half maximum parameter on the order of 80 ps. The average excitation power is 2 μW.
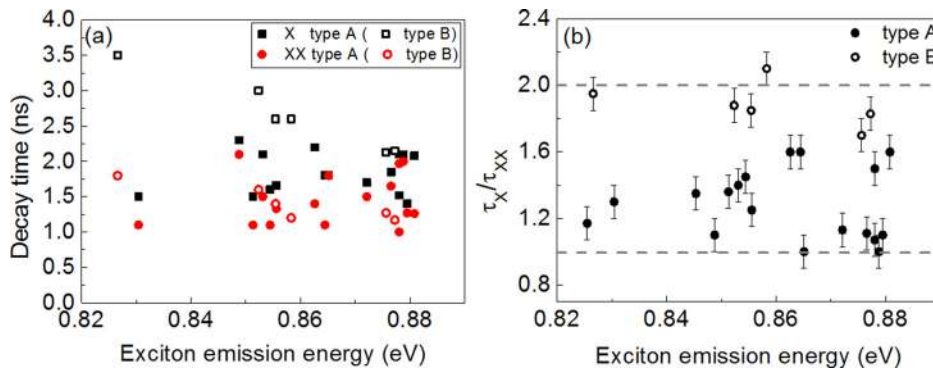
FIG. 3. (a) Exciton emission energy dependence of excitons and biexcitons decay times. Data points have been additionally divided into two group of lines corresponding to type A and B emitters [based on Fig. 4(a)]. (b) Exciton energy dependence of exciton to biexciton decay time ratio. With dotted grey lines extreme values of exciton to biexciton decay time ratio are presented, with ratios equal to 1 and 2. In (a), the size of the data points represents error bars.

To get a more general picture of the emission kinetics of the dashes, the μTRPL experiments have been repeated for more than 20 quantum dashes, which in general differ in size, shape, or chemical composition. One needs to mention that these parameters define the exciton and biexciton emission energies for each QDash.[29] We have derived a dependence of characteristic decay times as a function of emission energy for particular excitonic complexes. Figure 3(a) presents a scattered character of the exciton and biexciton PL lifetimes without actually any explicit dependence on the emission energy. While the exciton PL decay time (black square points) varies from 1.5 ± 0.1 ns up to 3.2 ± 0.1 ns, the biexciton one (red circles) changes between 1.0 ± 0.1 ns and 2.0 ± 0.1 ns, confirming a rather broad distribution of these parameters within the ensemble, and hence the natural significant inhomogeneity of the dashes.

A more systematic picture appears when the respective dependence of the τ_X/τ_{XX} ratio is plotted as a function of the emission energy, as in Fig. 3(b). Most of the registered τ_X/τ_{XX} values falls between approximately 1.2 ± 0.1 and 1.6 ± 0.1, whereas for several cases, the τ_X/τ_{XX} reaches more than 1.7 or gets close to 1. Therefore, the points in this dependence can be divided into two main groups: the ones with $\tau_X/\tau_{XX} < 1.6$, called "type A" QDashes, and the second one with $\tau_X/\tau_{XX} > 1.7$, named "type B" QDashes. The values typical for type A dashes suggest a weaker (intermediate) confinement regime. This experimental finding is in agreement with direct intuitive interpretation, even without detailed calculations. Large size of a QDash results in effective squeezing of the states' ladder in both the conduction and valence bands, where the level spacing can be below 25 meV and 10 meV,[30,34] respectively. It means that Coulomb and configuration interaction energies in QDashes (15–25 meV)[29] become comparable to the

confinement quantization energies, which thus strongly affect the emission kinetics of X and XX.

A bit more puzzling explanation of the confinement properties is expected for the type B QDashes, among which some exhibit the τ_X/τ_{XX} values closer to 2 (i.e., to the strong confinement regime). This, however, could be the result of a population of significantly shorter dashes within the strongly inhomogeneous ensemble, which can be found when looking at their morphologies.[25] Another reason could be shape or composition fluctuations, which can effectively reduce the spatial extension of the confinement potential, localizing charges in a much smaller volume than expected for a non-perturbed (or more uniform) QDash.[25] It needs to be stated that in the abovementioned localization case, also the linear polarization anisotropy of dash emission should be significantly reduced with respect to the structure without shape fluctuations.[25,35] The latter effect has been studied, both theoretically[35,36] and experimentally, on the ensemble of InAs/InAlGaAs/InP and InAs/InGaAsP/InP quantum dashes.[25] The data obtained here on the emission kinetics in single QDashes support the scenario with the existence of potential fluctuations in some of the QDash emitters.

Since the experimentally obtained biexciton binding energy expresses, in fact, the Coulomb interactions and configuration mixing[29,32] for the given system, which are also confinement dependent, we have plotted the relation between the τ_X/τ_{XX} ratio and the biexciton binding energy, shown in Fig. 4(a). The data for type A and B QDashes clearly segregate into two separated groups, in spite of no specific dependence between the biexciton binding energy and the emission energy [Fig. 4(b)]. The "type A" QDashes, recognized as the more typical ones, have rather large biexciton binding energies accompanied by a smaller τ_X/τ_{XX} ratio. For larger QDashes, all the Coulomb interaction components
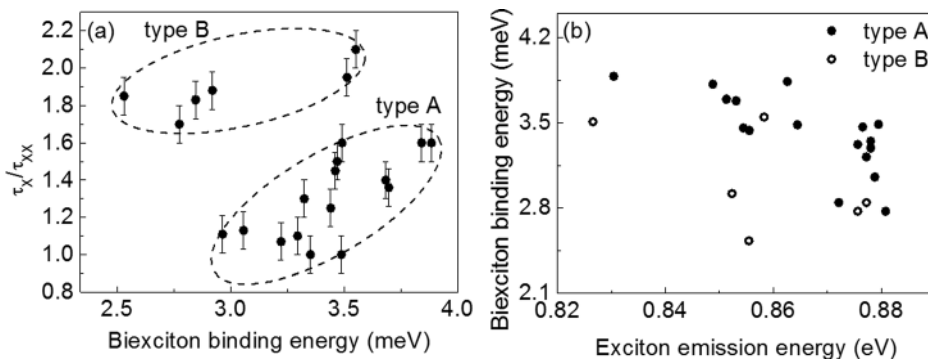

FIG. 4. (a) Biexciton binding energy vs. exciton to biexciton decay time ratio. Each point corresponds to μTRPL data obtained for a pair of exciton and biexciton lines identified as originating from the same QDash. Dotted lines segregate data points into two groups: type A and B emitters. (b) The exciton emission energy vs. the biexciton binding energy.

(electron-electron, hole-hole, and electron-hole) become smaller due to decreasing overlap integral between the respective wave functions in a larger object. However, for the InAs/InAlGaAs/InP(001) QDashes beside direct Coulomb interaction, the correlations and hence the states configuration mixing become important.[29] They make the biexciton state binding, whereas the Coulomb interaction exclusively would make the biexciton state unbinding. Here, the biexcitons are strongly binding, with absolute values of the binding energy on the order of 3–3.5 meV for the type A and 2.5–3.0 for the type B dashes. It might be related to interplay between the rising Coulomb interaction strength and weakening of the contribution from the wave function configuration mixing in smaller dashes.

In conclusion, in this experimental work, we made an attempt to understand the confinement regime in single self-assembled InAs/InAlGaAsP/InP(001) QDashes emitting around 1.5 μm through the analysis of the kinetic properties of exciton and biexciton states and their correlation to other experimentally obtained parameters, like exciton emission energy or biexciton binding energy. The experiments have been performed on a large number of emitters to get a more general picture. We have found that the majority of QDashes can be characterized by the intermediate rather than weak confinement limit with $1.2 \pm 0.1 < \tau_X/\tau_{XX} < 1.6 \pm 0.1$. This observation has been additionally supported by a relation between the biexciton to exciton decay rates' ratio and the biexciton binding energy. Those QDashes being in the intermediate confinement regime exhibit larger biexciton binding energy, falling into the range of 3.0–3.7 meV, as compared to the cases getting closer to the strong confinement, exhibiting the biexciton binding energy usually below 3 meV. It means that for a typical QDash, the Coulomb correlations are important and cannot be neglected as for small nanostructures in the strong confinement regime.

[1]I. Schwartz, D. Cogan, E. R. Schmidgall, Y. Don, L. Gantz, O. Kenneth, N. H. Lindner, and D. Gershoni, Science **354**, 434 (2016).
[2]R. Raussendorf and J. Harrington, Phys. Rev. Lett. **98**, 190504 (2007).
[3]T. Miyazawa, K. Takemoto, Y. Nambu, S. Miki, T. Yamashita, H. Terai, M. Fujiwara, M. Sasaki, Y. Sakuma, M. Takatsu, T. Yamamoto, and Y. Arakawa, Appl. Phys. Lett. **109**, 132106 (2016).
[4]M. Benyoucef, M. Yacob, J. P. Reithmaier, J. Kettler, and P. Michler, Appl. Phys. Lett. **103**, 162101 (2013).
[5]Ł. Dusanowski, M. Syperek, J. Misiewicz, A. Somers, S. Höfling, M. Kamp, J. P. Reithmaier, and G. Sęk, Appl. Phys. Lett. **108**, 163108 (2016).
[6]X. Liu, K. Akahane, N. A. Jahan, N. Kobayashi, M. Sasaki, H. Kumano, and I. Suemune, Appl. Phys. Lett. **103**, 061114 (2013).
[7]H.-Z. Song, M. Hadi, Y. Zheng, B. Shen, L. Zhang, Z. Ren, R. Gao, and Z. M. Wang, Nanoscale Research Letters **12**, 128 (2017).
[8]M. D. Birowosuto, H. Sumikura, S. Matsuo, H. Taniyama, P. J. van Veldhoven, R. Nötzel, and M. Notomi, Sci. Rep. **2**, 321 (2012).
[9]L. He, M. Gong, C. F. Li, G. C. Guo, and A. Zunger, Phys. Rev. Lett. **101**, 157405 (2008).
[10]K. Takemoto, Y. Sakuma, S. Hirose, T. Usuki, N. Yokoyama, T. Miyazawa, M. Takatsu, and Y. Arakawa, Jpn. J. Appl. Phys., Part 2 **43**, L993 (2004).
[11]D. Elvira, R. Hostein, B. Fain, L. Monniello, A. Michon, G. Beaudoin, R. Braive, I. Robert-Philip, I. Abram, I. Sagnes, and A. Beveratos, Phys. Rev. B **84**, 195302 (2011).
[12]J. H. Kim, C. J. K. Richardson, R. P. Leavitt, and E. Waks, Nano Lett. **16**, 7061 (2016).
[13]K. Takemoto, M. Takatsu, S. Hirose, N. Yokoyama, Y. Sakuma, T. Usuki, T. Miyazawa, and Y. Arakawa, J. Appl. Phys. **101**, 81720 (2007).
[14]Ł. Dusanowski, M. Syperek, P. Mrowiński, W. Rudno-Rudziński, J. Misiewicz, A. Somers, S. Höfling, M. Kamp, J. P. Reithmaier, and G. Sęk, Appl. Phys. Lett. **105**, 21909 (2014).
[15]K. Takemoto, Y. Nambu, T. Miyazawa, Y. Sakuma, T. Yamamoto, S. Yorozu, and Y. Arakawa, Sci. Rep. **5**, 14383 (2015).
[16]M. Paul, F. Olbrich, J. Höschele, S. Schreier, J. Kettler, S. L. Portalupi, M. Jetter, and P. Michler, Appl. Phys. Lett. **111**, 033102 (2017).
[17]J. Kettler, M. Paul, F. Olbrich, K. Zeuner, M. Jetter, and P. Michler, Appl. Phys. B **122**, 48 (2016).
[18]J. Kim, T. Cai, C. J. K. Richardson, R. P. Leavitt, and E. Waks, Optica **3**, 577 (2016).
[19]A. Kors, K. Fuchs, M. Yacob, J. P. Reithmaier, and M. Benyoucef, Appl. Phys. Lett. **110**, 31101 (2017).
[20]S. Frederick, D. Dalacu, D. Poitras, G. C. Aers, P. J. Poole, J. Lefebvre, D. Chithrani, and R. L. Williams, Microelectron. J. **36**, 197 (2005).
[21]J. Brault, M. Gendry, G. Grenet, G. Hollinger, Y. Desières, and T. Benyattou, Appl. Phys. Lett. **73**, 2932 (1998).
[22]L. González, J. M. García, R. García, F. Briones, J. Martínez-Pastor, and C. Ballesteros, Appl. Phys. Lett. **76**, 1104 (2000).
[23]A. Sauerwald, T. Kümmell, G. Bacher, A. Somers, R. Schwertberger, J. P. Reithmaier, and A. Forchel, Appl. Phys. Lett. **86**, 253112 (2005).
[24]N. Sritirawisarn, F. W. M. van Otten, T. J. Eijkemans, and R. Nötzel, J. Cryst. Growth **305**, 63 (2007).
[25]A. Musiał, P. Kaczmarkiewicz, G. Sęk, P. Podemski, P. Machnikowski, J. Misiewicz, S. Hein, S. Höfling, and A. Forchel, Phys. Rev. B **85**, 35314 (2012).
[26]Ł. Dusanowski, A. Musiał, A. Maryński, P. Mrowiński, J. Andrzejewski, P. Machnikowski, J. Misiewicz, A. Somers, S. Höfling, J. P. Reithmaier, and G. Sęk, Phys. Rev. B **90**, 125424 (2014).
[27]Ł. Dusanowski, M. Syperek, W. Rudno-Rudziński, P. Mrowiński, G. Sęk, J. Misiewicz, A. Somers, J. P. Reithmaier, S. Höfling, and A. Forchel, Appl. Phys. Lett. **103**, 253113 (2013).
[28]P. Mrowiński, A. Musiał, A. Maryński, M. Syperek, J. Misiewicz, A. Somers, J. P. Reithmaier, S. Höfling, and G. Sęk, Appl. Phys. Lett. **106**, 53114 (2015).
[29]P. Mrowiński, M. Zieliński, M. Świderski, J. Misiewicz, A. Somers, J. P. Reithmaier, S. Höfling, and G. Sęk, Phys. Rev. B **94**, 115434 (2016).
[30]A. Maryński, G. Sęk, A. Musiał, J. Andrzejewski, J. Misiewicz, C. Gilfert, J. P. Reithmaier, A. Capua, O. Karni, D. Gready, G. Eisenstein, G. Atiya, W. D. Kaplan, and S. Kölling, J. Appl. Phys. **114**, 94306 (2013).
[31]K. Ryczko, G. Sęk, and J. Misiewicz, J. Appl. Phys. **115**, 213502 (2014).
[32]M. Wimmer, S. Nair, and J. Shumway, Phys. Rev. B **73**, 165305 (2006).
[33]G. Narvaez, G. Bester, A. Franceschetti, and A. Zunger, Phys. Rev. B **74**, 205422 (2006).
[34]M. Syperek, Ł. Dusanowski, J. Andrzejewski, W. Rudno-Rudziński, G. Sęk, J. Misiewicz, and F. Lelarge, Appl. Phys. Lett. **103**, 83104 (2013).
[35]P. Kaczmarkiewicz and P. Machnikowski, Semicond. Sci. Technol. **27**, 105012 (2012).
[36]P. Kaczmarkiewicz, A. Musiał, G. Sęk, P. Podemski, P. Machnikowski, and J. Misiewicz, Acta Phys. Pol., A **119**, 633 (2011).